

GEM NEWS INTERNATIONAL

Contributing Editors
Gagan Choudhary, *IIGJ-Research & Laboratories Centre, Jaipur, India* (gagan.choudhary@iigjrlc.org)
Guanghai Shi, *School of Gemmology, China University of Geosciences, Beijing* (shigh@cugb.edu.cn)



Figure 1. Left to right: Three faceted colorless enstatites weighing 0.96, 1.15, and 1.55 ct. Photo by Jianxing Wang.

COLORED STONES AND ORGANIC MATERIALS

Fluorapatite inclusions in colorless enstatite. Enstatite ($Mg_2Si_2O_6$), a member of the pyroxene group, ranges in color from colorless and light green to deep brown. Most of the gem-quality material originates from Myanmar, Sri Lanka, and Tanzania (W. Schumann, *Gemstones of the World*, 4th ed., Sterling Publishing, New York, 2009).

The authors recently acquired three faceted colorless stones weighing 0.96, 1.15, and 1.55 ct (figure 1), identified as enstatite through Raman analysis. According to the seller, the samples were from Sri Lanka. Compared to colored enstatite, these specimens demonstrated lower refractive index, birefringence, and specific gravity. The measured refractive indices were n_α = 1.655–1.657, n_β = 1.659–1.660, and n_γ = 1.665, with a birefringence of 0.008–0.010 (biaxial positive), and a mean hydrostatic specific gravity of 3.23.

Ultraviolet/visible absorption spectroscopy showed an absorption peak at 505 nm. The absorption intensity was notably weaker than in green to brown varieties, likely reflecting lower iron content (P.C. Zwaan, "Enstatite, cordierite, kornerupine, and scapolite with unusual properties from Embilipitiya, Sri Lanka," Winter 1996 *G&G*, pp. 262–269). All three were inert to long-wave (365 nm) UV, while exhibiting weak to strong pale yellow fluorescence under short-wave (254 nm) UV.

In addition to the commonly reported internal features of enstatite—such as fluid inclusions (https://www.gia.edu/gia-gubelin-gem-project-research, collection no. 34820), acicular inclusions (J.I. Koivula et al., "Gemmological investigation of a large faceted east African enstatite," *Journal of Gemmology*, Vol. 21, No. 2, 1988, pp. 92–94), quartz inclusions (Zwaan, 1996), oriented tubes filled with

Editors' note: Interested contributors should send information and illustrations to gandgeditorial@gia.edu.

Gems & Gemology, Vol. 62, No. 3, pp. 308–320.

© 2026 Gemological Institute of America



Figure 2. Tiny fissures formed by pyroxene-related cleavages surround a fluorapatite inclusion in the 0.96 ct enstatite. Photomicrograph by Jianxing Wang; field of view 2.06 mm.

magnesite, and rutile inclusions responsible for asterism in star enstatite (Spring 2022 GNI, pp. 120–125)—the authors identified colorless, transparent mineral inclusions in all samples. Some inclusions were surrounded by tiny fissures formed by pyroxene-related cleavages (figure 2). Raman spectra collected with 532 nm excitation identified these mineral inclusions as fluorapatite, confirmed by the RRUFF database (figure 3; B. Lafuente et al., 2015, https://www.rruff.net/wp-content/uploads/2023/04/HMC1-30.pdf).

Jianxing Wang
Jewelry Testing Center
Shenzhen Polytechnic University, China

Figure 3. Raman spectra of the fluorapatite inclusions in the three enstatite samples, collected with 532 nm excitation, compared to a RRUFF reference spectrum. Spectra are offset vertically for clarity.

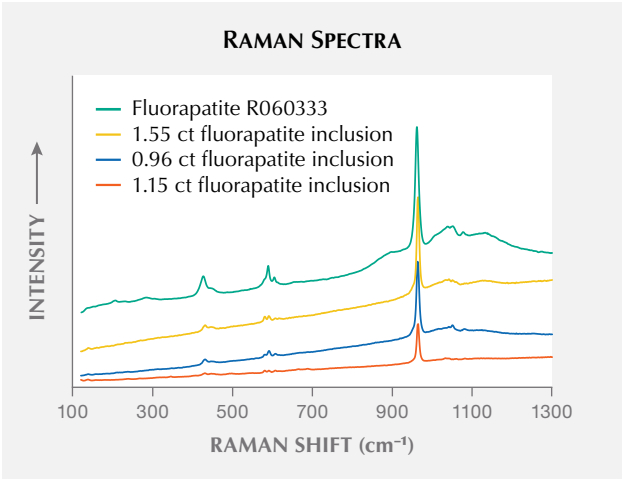

Kong Gao
Jewelry Institute
Guangzhou Polytechnic University, China

Boyue Chen
School of Gemmology
China University of Geosciences, Beijing

Grossular garnet with green halo inclusions. The Laboratoire Français de Gemmologie (LFG) received for analysis a 5.09 ct slightly yellowish green cushion-cut gem that was notable for its prominent bright green internal "spots" (figure 4). These nearly spherical halos exhibited a grainy

Figure 4. This 5.09 ct slightly yellowish green cushion-cut grossular garnet features conspicuous green nearly spherical halos. Photos by Thiala Magalhaes.

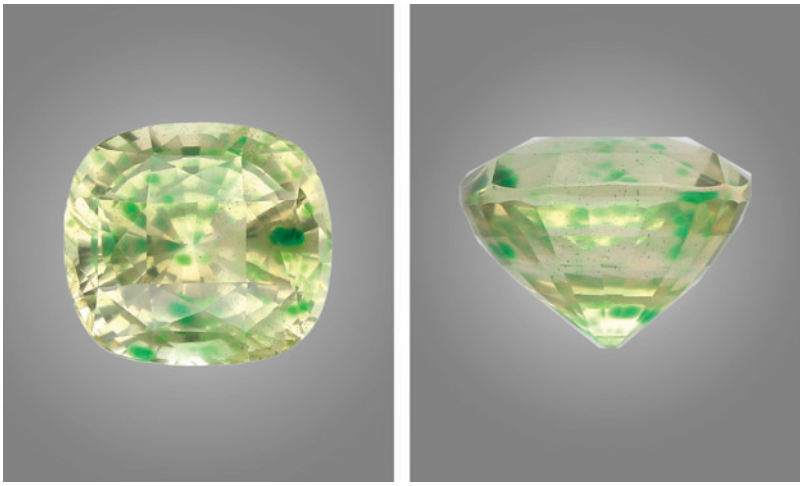

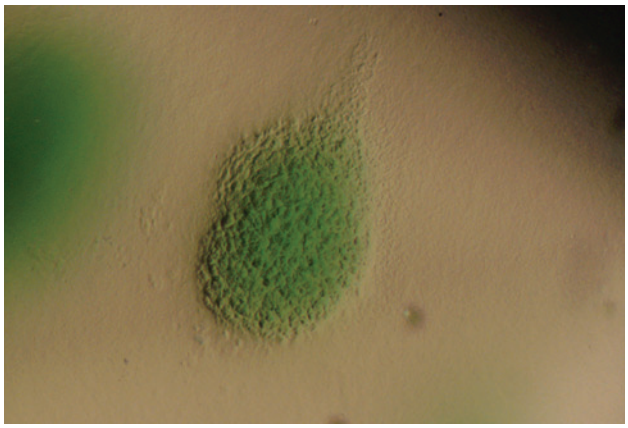

Figure 5. Detail of the green halos, which display an irregular, grainy appearance. Photomicrograph by Aurélien Delaunay; field of view ~1.78 mm.

structure (figure 5) and well-defined borders. At least two of the halos contained central black inclusions (figure 6, left); it is possible that the remaining spots also contained a central black core that was hidden by the relatively opaque green layer. Viewed between crossed polarizers, the green areas appeared slightly birefringent (figure 6, right).

The stone's refractive index of 1.735 and specific gravity of 3.53 were consistent with grossular garnet, and its identity was confirmed by vibrational spectroscopy. Raman analysis revealed two main peaks at approximately 881 and 375 cm^{-1}, corresponding to the characteristic features of grossular. Infrared transmission spectroscopy further corroborated this identification. The OH region contained the same features between 3500 and 3700 cm^{-1} as those for a grossular garnet sample from Tanzania on the Caltech Mineral Spectroscopy Server (http://minerals.gps.caltech.edu/FILES/Infrared_OH/GARNET/gt771.gif). Finally, energy-dispersive X-ray fluorescence chemical analysis of the table revealed silicon, calcium, and aluminum as principal components—62.17, 24.09, and 12.36 wt.% oxide, respectively—corresponding to grossular garnet's chemical formula of $Ca_3Al_2(SiO_4)_3$. Minor and trace impurities detected included magnesium (0.68 wt.% oxide), iron (0.61 wt.% oxide), chromium (0.04 wt.% oxide), and manganese (0.02 wt.% oxide).

The grossular's green color was likely caused by chromium (isolated Cr^{3+}), which is supported by the presence of chromium and comparison with chrome-bearing grossular of the same color. The only locality known to produce grossular containing green patches, or spherical halos, is the Jeffrey mine in Val-des-Sources (formerly Asbestos) in southeastern Quebec, Canada (R. Williams and J.D. Grice, "Famous mineral localities: The Jeffrey mine, Asbestos, Québec," *Mineralogical Record*, Vol. 10, No. 2, 1979, pp. 69–80). The black inclusions observed in those crystals were identified as chromite ($Fe^{2+}Cr_2O_4$; Williams and Grice, 1979), which explains the presence of chromium. This suggests that the dark inclusions observed in the present sample are chromite as well.

At 9.86 mm in its longest dimension, the size of the submitted gem is exceptional. Previously reported crystals with black cores and green halos did not exceed 1.5 cm (Williams and Grice, 1979; M. Amabili et al., "Recent discoveries at the Jeffrey mine, Asbestos, Québec," *Mineralogical Record*, Vol. 35, No. 2, 2004, pp. 123–135; L. Horváth et al., "The Jeffrey mine, Asbestos, Québec, Canada," *Mineralogical Record*, Vol. 44, No. 4, 2013, pp. 375–417). The presence of multiple green halos is also unusual; the crystals described in the literature had only one central spot (Horváth et al., 2013).

Observation suggests that chromium may have leaked or diffused from the central dark spot, presumably chromite, to create the green halo. No theory has been proposed for this curious geometric distribution. The highest chromium concentration measured in a green halo was less

Figure 6. Left: This green halo has black crystals in its center. Right: The same halo viewed between crossed polarizers, indicating strained, anisotropic zones. Photomicrographs by Aurélien Delaunay; field of view ~2.8 mm.

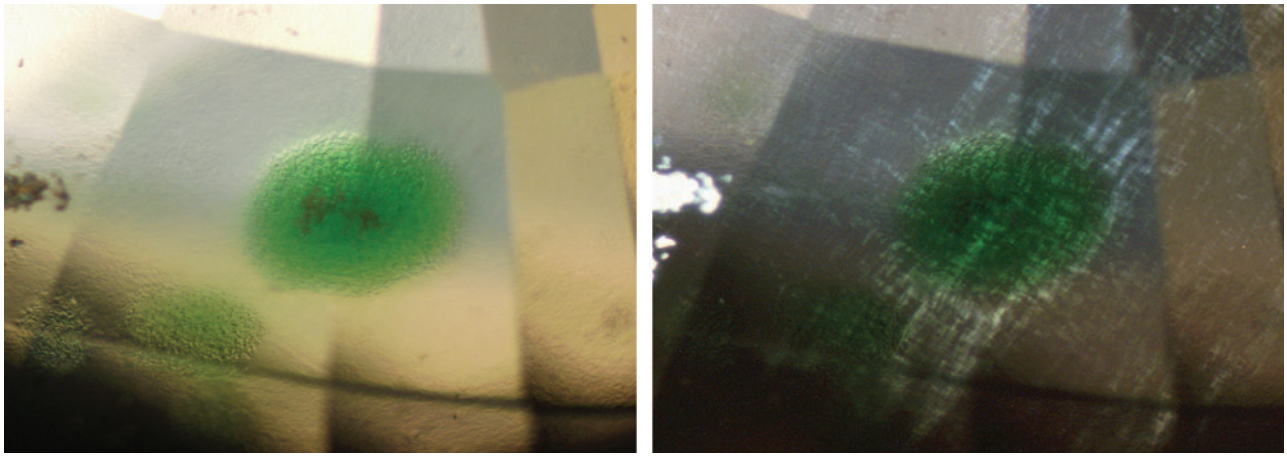



Figure 7. A 128.99 ct polished quartz (left) and a 1410.0 g rough quartz (right), both containing yellow to greenish yellow inclusions. Photos by Liyan He (left) and Wang Zhang (right).

than 9 wt.% Cr_2O_3, which corresponds to about 25 wt.% uvarovite, so the green zone cannot be classified as uvarovite (Horváth et al., 2013). Overall, the unique combination of characteristics makes this a desirable collector gem.

Aurélien Delaunay and Ugo Hennebois
Laboratoire Français de Gemmologie (LFG)
Paris, France

Emmanuel Fritsch
Nantes Université, Nantes, France

Stefanos Karampelas
Aristotle University of Thessaloniki, Greece

Sulfur inclusions in quartz. The authors recently examined two Zambian quartz samples: a 128.99 ct polished specimen and a 1410.0 g rough, each containing a series of yellow to greenish yellow inclusions (figure 7). These inclusions ranged from transparent to translucent, were inert to long- (365 nm) and short-wave (254 nm) ultraviolet radiation, and did not exhibit dichroism. In the polished sample, the inclusions occurred along cracks in the host quartz, suggesting that they crystallized after the quartz formed (figure 8, left). In the rough sample, the inclusions were better crystallized, with a group of grains displaying subhedral morphology and a greasy luster (figure 8, right).

Figure 8. Left: The sulfur inclusions in the polished quartz sample crystallized along the cracks. Photomicrograph by Liyan He; field of view 9.8 mm. Right: A group of sulfur grains in the rough sample, exhibiting subhedral morphology, transparency, and a greasy luster. Photomicrograph by Wingtak Lui; field of view 7.8 mm.



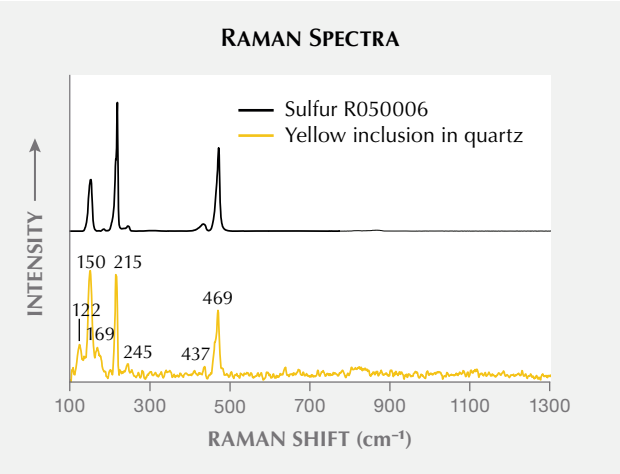

Figure 9. Comparison of the Raman spectrum (532 nm laser excitation) of a representative sulfur inclusion and the RRUFF reference spectrum for sulfur. Spectra are offset vertically for clarity.



Figure 10. The author interviews George Harlow in the Allison and Roberto Mignone Hall of Gems and Minerals at the AMNH in New York City. Photo by Pedro Padua.

Raman spectra collected from inclusions in both samples featured major peaks at approximately 149, 215, and 469 cm^{-1} and minor peaks at 121, 168, 244, and 437 cm^{-1}, consistent with the RRUFF reference spectrum for sulfur (figure 9; B. Lafuente et al., 2015, https://www.rruff.net/wp-content/uploads/2023/04/HMC1-30.pdf). Pure elemental sulfur is relatively uncommon; most native sulfur is biogenically produced or associated with sedimentary and volcanic activity. Yellow sulfur is temperature sensitive and occurs in two crystalline forms: orthorhombic (α-sulfur, stable below approximately 96°C) and monoclinic (β-sulfur, which α-sulfur transitions into around 96°C and melts at approximately 119°C). As temperature increases, sulfur begins to melt or turns orange and red and becomes amorphous (A.V. Tobolsky and A. Eisenberg, "Equilibrium polymerization of sulfur," *Journal of the American Chemical Society*, Vol. 81, No. 4, 1959, pp. 780–782; G. Kutney, *Sulfur: History, Technology, Applications & Industry*, ChemTec Publishing, 2007, 260 pp.). The temperature sensitivity of sulfur makes these inclusions in quartz unique.

Liyan He
Guangdong Gemstones & Precious Metals Testing Center
Guangzhou, China

Wang Zhang and Wingtak Lui
Min De Minerals & Gem Research Co., Ltd.
Nanjing, China

Interview with George Harlow, gem curator at the American Museum of Natural History. George Harlow, curator emeritus in the Department of Earth and Planetary Sciences at the American Museum of Natural History (AMNH) in New York City, has been instrumental in shaping the museum's globally renowned gem and mineral collections for the past 50 years. Since its first exhibits went on display in 1871, AMNH has preserved significant scientific collections for research and public education. Its physical sciences collection now contains more than 110,000 minerals and gems, including volcanic rocks from Vesuvius and Martian meteorites. An oral history interview with Harlow (figure 10) was conducted at the Allison and Roberto Mignone Hall of Gems and Minerals, a centerpiece of the museum.

George Harlow, born on March 8, 1949, in Paterson, New Jersey, was introduced to geology by his eighth-grade science teacher, who inspired him to explore. He recalls conducting weathering experiments with feldspars and exploring feldspar outcroppings in Connecticut. At Harvard, Professor Stephen Norton opened his eyes to geology and mineralogy, and Harlow decided to major in geology. For his senior thesis, he grew

Figure 11. Harlow holds a Verneuil synthetic spinel he grew as a student at Harvard in 1971. Photo by Pedro Padua.



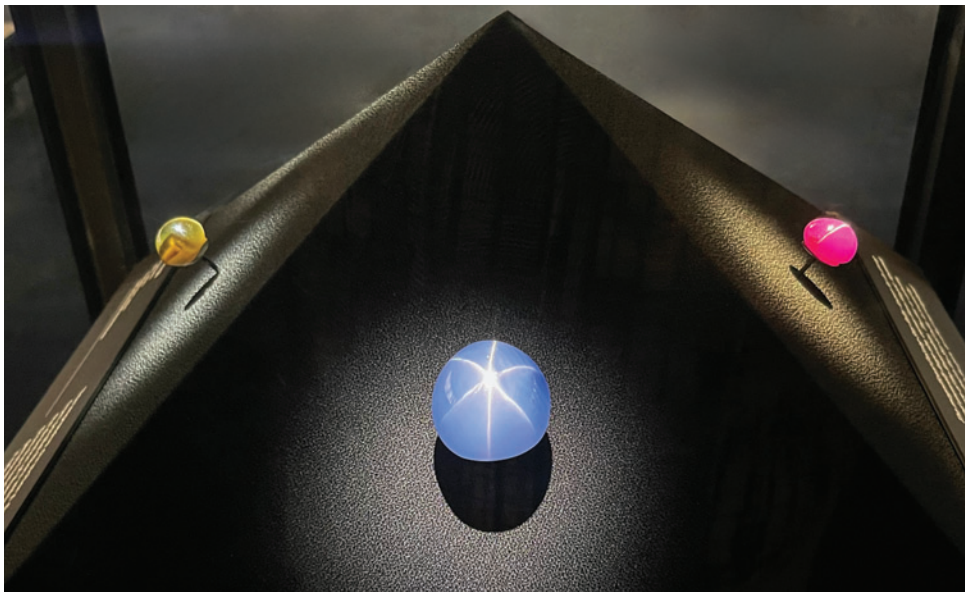

Figure 12. The 563.35 ct Star of India star sapphire, one of the largest in the world, is notable for its almost flawless quality and unusual asterism on both sides of the stone. Photo by Pedro Padua; courtesy of the American Museum of Natural History.

Verneuil synthetic spinel (figure 11), and he went on to graduate *magna cum laude*.

After obtaining his PhD from Princeton University, Harlow joined AMNH in 1976 as curator of the gem and mineral collection. Harlow describes exploring its vast treasures (figure 12) as "just magic for me." Harlow sees himself as a detective seeking to unravel the processes that create gem materials. He says that all "raw materials" have a story, and our role is to understand how the earth has created them. He curated the Hall of Gems and Minerals, which contains more than 5,000 specimens from 98 countries, to showcase how scientists classify gems and how they are used for personal adornment, tools, and technology (figure 13).

While Harlow has a quiet passion for educating museum visitors, his particular field of research has been jadeite jade—a rare and unusual material with only 20 occurrences worldwide. Jadeite is one of a handful of sodium aluminum silicate minerals, most of which are not dense and have open structures. Jadeite jade is the densest, a result of its formation deep in the earth, perhaps 50–60 km below the surface.



Figure 13. An AMNH display of crystals and rocks, demonstrating the classifications of gems and how these materials are used in both historical and modern contexts. Photo by Pedro Padua; courtesy of the American Museum of Natural History.

Initially drawn to jadeite jade carvings and wondering how artisans found such large pieces to work with, Harlow became interested in jadeite jade's origins. Working with a graduate student who was interested in the relationship between the jades of Asia and those of the New World, Harlow conducted noteworthy field studies in Guatemala. In the 1960s, the Guatemalan jadeite jade source was thought to be around 10 km long, but after spending collectively more than a year on the ground, their fieldwork extended that known source to more than 200 km long. The research also led to new information on other minerals found in Guatemala, such as members of the serpentine mineral group. Harlow spoke about the incredible experience of being surrounded by these materials in the museum, going into the field, bringing back new materials for study, and adding them to the AMNH collection. He estimates that he has contributed more than 2,500 objects from Guatemala.

Harlow has also taught graduate courses in crystallography and crystal chemistry at Princeton and Columbia University, led local field trips, and lectured extensively. He is the author or coauthor of 134 books and articles on gemstones and minerals, along with nearly 200 abstracts of presentations to various scientific groups. His research has long supported the assertion that the sources of many gems can be identified by analyzing their geological context and distinctive trace element contents.

In the 1980s, Harlow turned his attention to diamonds, drawn to their dazzling beauty and the secrets they reveal about Earth's core. "These tiny inclusions inside them," he marvels, "record the diamond's incredible journey." Collaborating with a colleague, he pursued an ambitious research and exhibition project. By the early 1990s, he knew he had stumbled upon "a great story." But he had to wait for the right moment to share the story of diamonds with the world; apartheid had to end first, since South Africa was the source of many legendary diamonds.

Harlow envisioned a diamond exhibition like no other, assembling breathtaking diamond jewelry steeped in history and intrigue, such as the glittering crown of Peter the Great, on loan from the Kremlin, alongside the 287 ct Tiffany diamond. Rare masterpieces from Van Cleef, Cartier, and other legendary jewelers would shimmer beside Renaissance art of nobles adorned in early diamond jewelry pieces. Harlow imagined more than just a static display; he wanted to bring the art of diamond cutting alive. A live diamond cutter would enthrall visitors, revealing the skill and craftsmanship behind transforming a rough stone into a brilliant gem as Harlow's "great story" came to life. Another standout attraction was colored diamonds, highlighted by the 260-gem display of the Aurora Collection.

The opening gala for Harlow's landmark *Nature of Diamonds* exhibition in New York (1997–1998) was such a must-attend event that tickets were being scalped. Due to its success, the exhibition was showcased at other museums. Vince Manson, his predecessor at AMNH, brought it to the San Diego Natural History Museum. From there, the exhibition went to Japan, where it drew half a million visitors in six weeks.



Figure 14. From the Ice Cold *exhibition, this diamond necklace was made by Jewelry Unlimited for Atlanta-based record label Quality Control Music. Photo by Pedro Padua; courtesy of the American Museum of Natural History.*

Nature of Diamonds helped raise awareness of the AMNH's role in research and education and led to other jewelry-centric exhibitions, such as *Pearls* (2002) and *Gold* (2006–2007). It also led to a rotating "maestro" gallery of unique exhibits, which continue to draw crowds. *Ice Cold* (2024–2025) was on display during the interview, highlighting the evolution of hip-hop jewelry over the past five decades (figure 14).

Harlow became curator emeritus of the AMNH's Department of Earth and Planetary Sciences in 2021. Through decades of research, teaching, and public engagement, George Harlow has advanced the scientific understanding of gem materials while transforming the AMNH's mineral collections into a resource of international significance.

This August 2024 interview was recorded on video as part of GIA's Oral History Project, to be used by future historians. Visit www.gia.edu/gems-gemology/fall-2026-gemnews-george-harlow to see more.

Al Gilbertson
GIA, Carlsbad



Figure 15. Left to right: Faceted hydrothermally grown aquamarine weighing 1.06, 1.01, and 1.03 ct. Photos by Jianxing Wang.

SYNTHETICS AND SIMULANTS

Unique ferberite inclusions in hydrothermal synthetic aquamarine. The authors recently examined a suite of seven oval brilliant-cut aquamarines from the Hong Kong Jewellery Show. The reseller reported these specimens were hydrothermal synthetic aquamarine. To the unaided eye, the samples were visually indistinguishable from natural aquamarine. Each stone weighed approximately 1 ct and measured about 6 × 8 mm, exhibiting a grayish blue to pale blue hue, vitreous luster, refractive index of 1.572–1.580, and specific gravity of approximately 2.75.

Three representative samples were chosen for detailed study (figure 15). Microscopic examination revealed the presence of seed crystals, slag-like inclusions, and distinct growth banding (figure 16). Infrared (IR) spectroscopy confirmed the host material as beryl and detected molecular water, consistent with the IR characterization approach for hydrothermal synthetic blue beryl documented by Adamo et al. (I. Adamo et al., "Aquamarine, Maxixe-type beryl, and hydrothermal synthetic blue beryl: Analysis and identification," Fall 2008 *G&G*, pp. 214–226). That study explained mid-IR spectroscopy, specifically the detection of water by absorption bands in the 4000–3400 cm^{-1} region, thus distinguishing it from flux-grown origin. The combined gemological, microscopic, and spectroscopic characteristics confirmed that the samples were hydrothermal synthetic aquamarine.

A particularly notable feature was that, during the early stages of crystal growth, a dense layer of brown inclusions formed on the seed crystal face (figure 17), resembling a patch of dark grass. The inclusions were opaque and exhibited a submetallic to metallic luster, predominantly occurring as tabular crystals, some of which aggregated into snowflake-like clusters.

Some of the inclusions were exposed on the facet surfaces, allowing Raman spectroscopic analyses to be conducted at multiple points using 785 nm laser excitation.

Figure 16. In this sample, the seed crystal is seen in the pavilion. Dark slag-like inclusions formed initially at the seed overgrowth interface, and distinct growth banding is also visible. Photomicrograph by Kong Gao; field of view 5.94 mm.

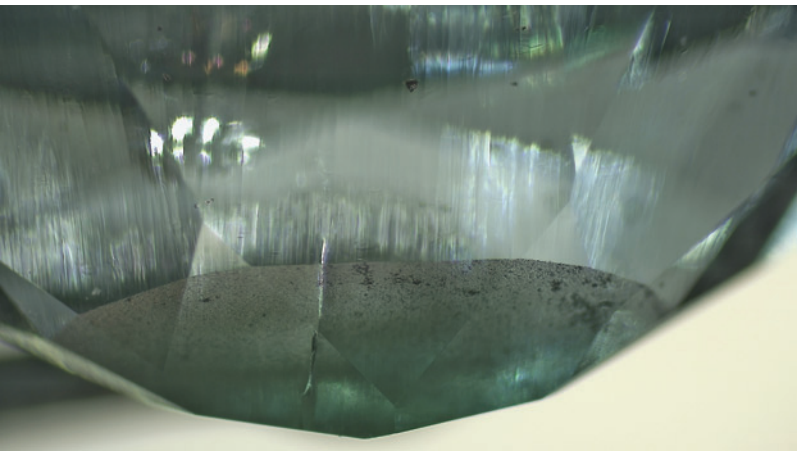

Figure 17. A dense layer of brown inclusions along the early growth interface. The seed crystal is visible at the junction between the kite facet and the star facet. Photomicrograph by Kong Gao; field of view 1.73 mm.



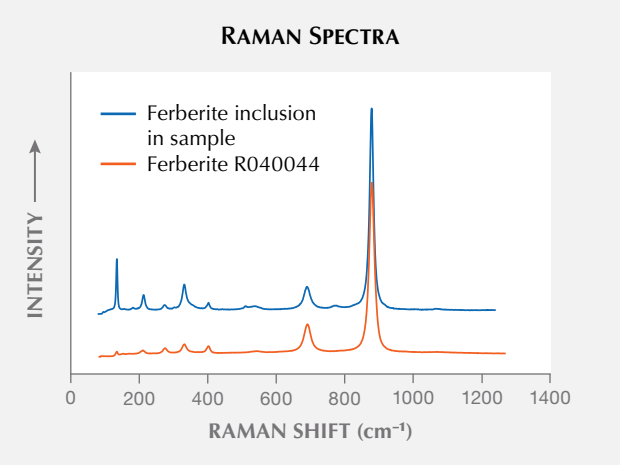

Figure 18. Raman spectrum using 785 nm laser excitation of a ferberite inclusion in a hydrothermal synthetic aquamarine sample, compared with a reference spectrum from the RRUFF database. Spectra are offset vertically for clarity.

As shown in figure 18, the representative spectrum closely matched that of ferberite ($FeWO_4$) when compared with reference data from the RRUFF database (B. Lafuente et al., 2015, https://www.rruff.net/wp-content/uploads/2023/04/HMC1-30.pdf). Complementary energy-dispersive X-ray fluorescence analyses further corroborated this identification; trace tungsten was detected exclusively at inclusion exposure sites, whereas adjacent inclusion-free areas showed no detectable tungsten signal.

To the authors' knowledge, this is the first documented occurrence of ferberite inclusions in hydrothermal synthetic aquamarine. Although previous studies on hydrothermal synthetic beryl have provided information on growth textures, fluid inclusions, and seed plates (e.g., J.E. Shigley et al., "Hydrothermal synthetic red beryl from the Institute of Crystallography, Moscow," Spring 2001 *G&G*, pp. 42–55; I. Adamo et al., "Characterization of the new Malossi hydrothermal synthetic emerald," Winter 2005 *G&G*, pp. 328–338), documented occurrences of solid inclusions have been restricted to phenakite, metals, and possible hematite platelets (e.g., R.E. Kane and R.T. Liddicoat, Jr., "The Biron hydrothermal synthetic emerald," Fall 1985 *G&G*, pp. 156–170; K. Schmetzer, "Hydrothermally grown synthetic aquamarine manufactured in Novosibirsk, USSR," Fall 1990 *G&G*, pp. 206–211).

The formation of ferberite is likely attributable to tungsten-bearing components in the autoclave, particularly tungsten heat shields. These may have released trace tungsten into the mineralizing solution through extended autoclave operation or localized corrosion. During crystal growth, dissolved tungsten would have combined with iron ions in the solution to form ferberite inclusions.

Jianxing Wang
Jewelry Testing Center
Shenzhen Polytechnic University, China

Kong Gao
Jewelry Institute
Guangzhou Polytechnic University, China

TREATMENTS

An antique-style jade carving with misleading surface characteristics. A square columnar carving with a cylindrical bore, measuring 15 × 15 × 39 mm (figure 19, left), was recently submitted to the National Center of Quality Inspection and Testing on Gold-Silver Products (NGGC) for identification. Carvings of this form, known as *yu cong* in Chinese, were produced mainly during the late Neolithic and early Bronze Ages for ritual purposes. The specimen's pale grayish green bodycolor, along with a mottled appearance caused by a whitish patina layer and white

Figure 19. Left: The submitted square columnar carving with a cylindrical bore, known as yu cong *in Chinese. Courtesy of Shuochao Gu. Right: The white corrosion spots on the surface are open pits (yellow arrows) and round near-surface inclusions (blue arrows). Photos by Bowen Zhao; field of view 3.66 mm (right).*



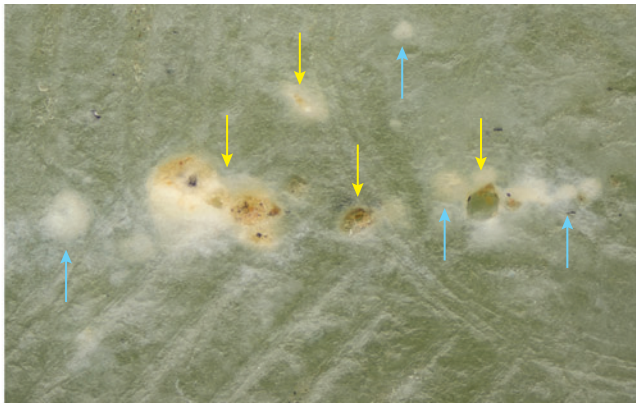

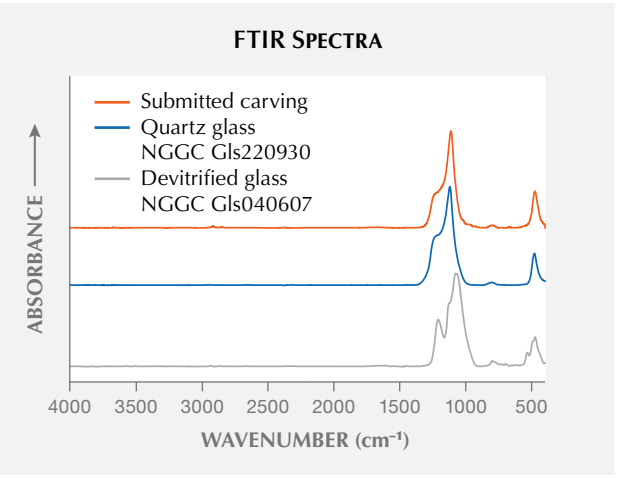



Figure 20. The infrared reflectance spectrum in the fingerprint region of the carving's surface closely matched quartz glass but differed from devitrified glass, whose texture (top right) can closely resemble that of nephrite jade (bottom right), as exhibited by the submitted carving. Photos by Bowen Zhao. A K-K transform was applied to the reflectance spectra collected. Spectra are offset vertically for clarity.

corrosion spots on the surface, created an initial impression of an ancient nephrite jade artifact.

Infrared reflectance spectroscopy, however, revealed the fingerprint absorption pattern of amorphous silica, indicating the material was either quartz glass or opal (figure 20, left). The measured refractive index of 1.45 supported this interpretation. Due to the carving's hollow interior, hydrostatic specific gravity testing was not applicable.

Microscopic examination showed the white corrosion spots were irregular or round micro pits filled with white waxy substances likely introduced during or after polishing. Some round white inclusions were observed just beneath the surface (figure 19, right). Their resemblance to the pits suggested that the pits were white inclusions exposed on the surface during the carving process. The round shape of pits and inclusions is typically associated with bubbles in glass.

Up to this point, all evidence pointed to a glass carving, with two exceptions. First, artificial devitrified glass can mimic the porridge-like texture of natural nephrite jade, but its texture is isotropic—unlike this carving's slightly oriented porridge-like texture (figure 20, right), which usually indicates nephrite from Xinjiang, China. Furthermore, the infrared fingerprint spectrum of artificial devitrified glass significantly differs from that of quartz glass (again, see figure 20, left).

Additional examinations were conducted to gather more evidence. On the carving's surface, the whitish patina layer showed weak whitish fluorescence under 370 nm ultraviolet light, while the grayish green matrix material remained inert. Raman spectra collected from multiple fluorescence-inert areas corresponding to the matrix consistently matched the pattern for tremolite. Meanwhile, the infrared transmittance spectrum in the 3000–8000 cm^{-1} range exhibited the characteristic hydroxyl absorptions of nephrite jade (figure 21). These findings confirmed the presence of a nephrite component in the carving yet appeared to contradict the earlier results, creating a paradox. One possible explanation, considering persistent rumors that some jade simulants are made by mixing jade powder with a

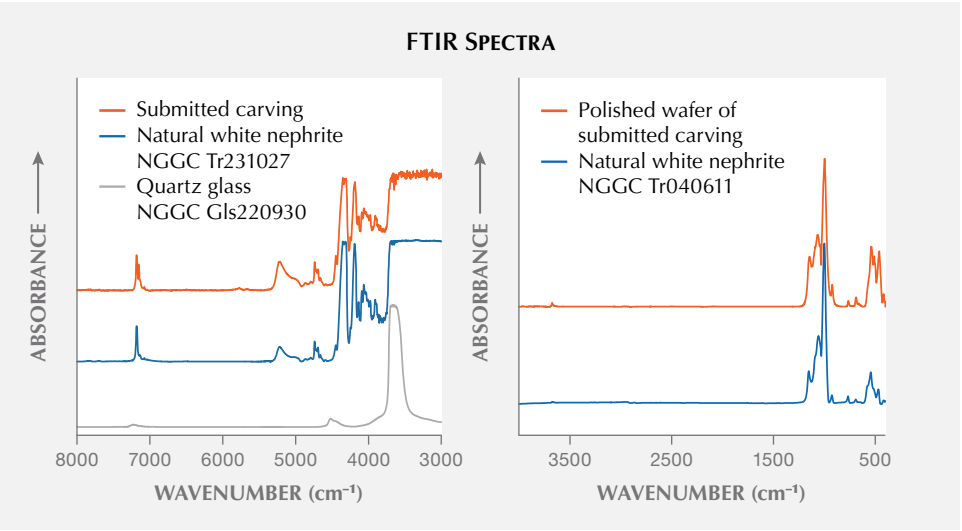

Figure 21. Left: The infrared transmittance spectrum of a polished wafer from the submitted carving was identical to that of a reference spectrum for nephrite, while the absorption features of quartz glass were absent. Right: The infrared reflectance spectrum of the carving's interior component also matched the fingerprint of nephrite. A K-K transform was applied to the reflectance spectra. Spectra are offset vertically for clarity.

cementing agent, was that the carving was made of glass mixed with a minor amount of nephrite powder. This hypothesis seemed to explain the results thus far, but it was insufficient to support a confident conclusion.

With the owner's permission, two polished wafers and two thin sections were sliced from the carving. The infrared reflectance spectrum of one of the polished wafers showed a nephrite pattern exclusively (figure 21), and magnification of the thin sections using cross-polarized light revealed a texture of fine fibrous tremolite interspersed with tremolite phenocrysts, while no optically isotropic substance such as glass was observed (figure 22). The carving was finally confirmed to be solid natural nephrite, leaving only the question of what caused the abnormal surface features.

It is well known that antique-style jade objects are sometimes artificially aged using calcination or chemical corrosion. Because tremolite decomposes into calcium-magnesium pyroxenes (typically diopside and enstatite) when heated above 900°C, this nephrite carving was more likely treated by chemical corrosion. An acidic solution can extract calcium and magnesium from the surface of nephrite, leaving a silica-rich layer that appears chalky and matte and exhibits whitish fluorescence. In all previous cases at NGGC, the surface of an aged nephrite object—whether naturally or artificially aged—had never been so thoroughly corroded and transformed into silica, and thus their infrared reflectance spectra had always retained a nephrite pattern (with slight spectral distortion due to surface structure degradation often observed).

The present case raises a clear warning that aging treatments for nephrite jade objects can completely alter the mineral composition at and near the surface, resulting in a series of gemological and spectral features that could mislead even experienced gemologists relying on nondestructive testing methods.

Figure 22. Magnification of the thin sections using cross-polarized light revealed a texture composed of tremolite phenocrysts and fine fibers. No optically isotropic glass was observed in the thin sections. Photomicrograph by Bowen Zhao; field of view 4.18 mm.

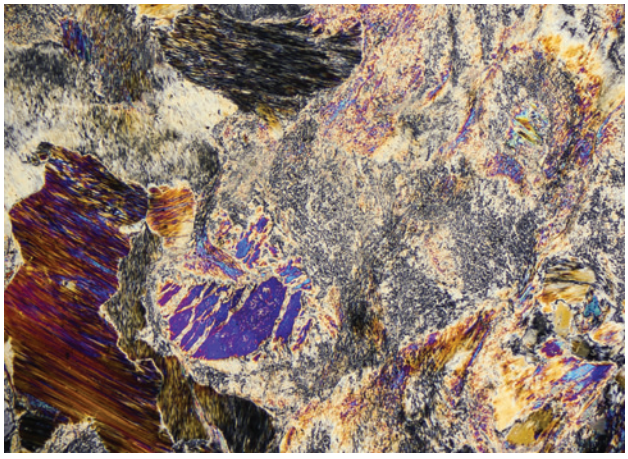

Bowen Zhao, Dingying Chen, and Weiji Qian
National Center of Quality Inspection and Testing on Gold-Silver Products (NGGC), Shanghai

Yuchen Zhang
Zhong Bao Center of Gem and Jade Identification, Shanghai

CONFERENCE REPORTS

New grading system launched at Turquoise United 2026. After a one-year hiatus, the Turquoise United conference returned to Albuquerque, New Mexico, in August 2026 with major announcements for the turquoise industry. Organized by Jacob and Joe Dan Lowry of the Turquoise Museum, the event seeks to unite the turquoise community, connecting dealers, artists, researchers, and collectors and providing opportunities to discuss topics of shared interest. The event marked the public launch of the Turquoise Standard, a grading system aimed at consistently evaluating the quality of natural turquoise.

The inaugural Turquoise United conference in 2022 (Fall 2022 GNI, pp. 390–394) featured a panel discussion on Joe Dan Lowry's proposed turquoise grading system. This year, the Lowrys presented updates on the grading system at multiple symposium sessions. The system assesses natural untreated turquoise cabochons using three quality factors, which have remained unchanged since the initial proposal: color, matrix, and "zat," a rating related to the visual impact of a stone. Each factor is evaluated individually against a master stone set for direct comparison.

Against a neutral background, each stone is compared with a master stone set for its color (blue, green-blue, blue-green, or green) and assigned a numeric grade from 0 (lowest grade) to 70 (most ideal color grade). Master stones represent each 5-point increment. Only stones in the blue category can receive scores higher than 50, as green hues deviate further from turquoise's ideal chemical composition.

Jacob noted that matrix and zat are now graded using letter scores ranging from D to V (figure 23). Flawless stones (no presence of matrix) are assigned a matrix letter grade by size (measured across the widest point; >11 mm gets the highest grade), reflecting the rarity of large, matrix-free specimens. Matrix grades for stones with matrix are determined by factors such as symmetry, cell size, spacing, and consistency. According to the grading system, a stone receiving the highest grade of D exhibits matrix that "forms a perfect spiderweb with maximum symmetry, refinement, and flawless balance. Structure, cell size, spacing, and distribution show few detectable inconsistencies." Therefore, a large flawless stone and a stone with a perfectly balanced spiderweb pattern could both receive the highest matrix grade. A low matrix score of V, meanwhile,

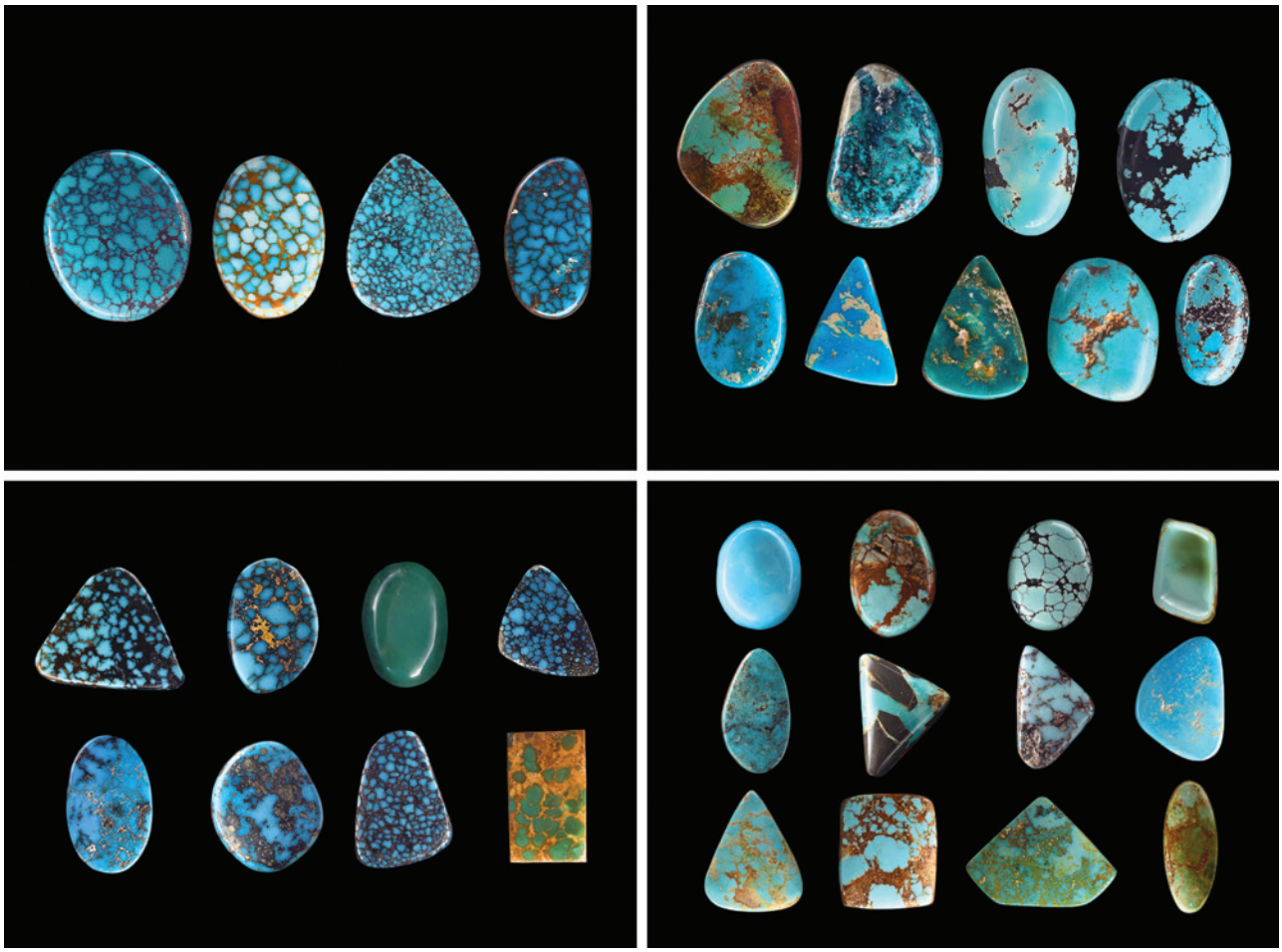

Figure 23. Top: Master stone sets for matrix grades F (left) and R (right). Bottom: Master stone sets for zat grades F (left) and R (right). Note that official grading is only conducted using the full master stone set, not the images. Courtesy of the Turquoise Standard.

indicates an "incidental, irrelevant, or dominating [matrix] with no recognizable structure or pattern." An instructional booklet including these descriptions was distributed to conference attendees.

Zat is the third and most difficult quality factor to define, combining the stone's contrast, vibrancy, and turquoise-matrix interaction. The term has appeared in descriptions of turquoise for more than a century (J.E. Pogue, *The Turquoise: A Study of Its History, Mineralogy, Geology, Ethnology, Archaeology, Mythology, Folklore, and Technology,* Memoirs of the National Academy of Sciences, Washington, D.C., 1915, 163 pp.). Cohesive, balanced, and intense patterns receive high zat scores on the D–V scale. Both matrix and zat are compared with dedicated master stone sets representing two-letter intervals (again, see figure 23); the letter grade in between the master stone intervals may be assigned if a stone falls between master stone properties.

Each submitted stone receives one numeric grade for color and separate letter grades for matrix and zat. Grading must be conducted through direct comparison to the master stone set by three trained graders who independently evaluate each stone and compare results. In cases of disagreement, each grader performs a second independent evaluation. If the grades still do not match, the graders jointly reexamine the specimen and the master stones while discussing the discrepancy. After reaching consensus, the official grades for color, matrix, and zat are assigned and recorded on an official report (figure 24).

In a symposium session at this year's conference, Jacob presented the results of a multi-year study evaluating the grading system's viability, including details about the methodology. The system was assessed using two groups to determine the consistency of results. The first group included five members of the turquoise industry who were provided with grading instructions and 57 stones to grade. The second group of eight gemological professionals with no specialized background in turquoise received a 15-minute overview of the system prior to grading the same set of stones. Both groups ordered the stones similarly, and the second group performed more consistently than the first, indicating that in-depth turquoise knowledge is not required to properly implement the grading system using the master

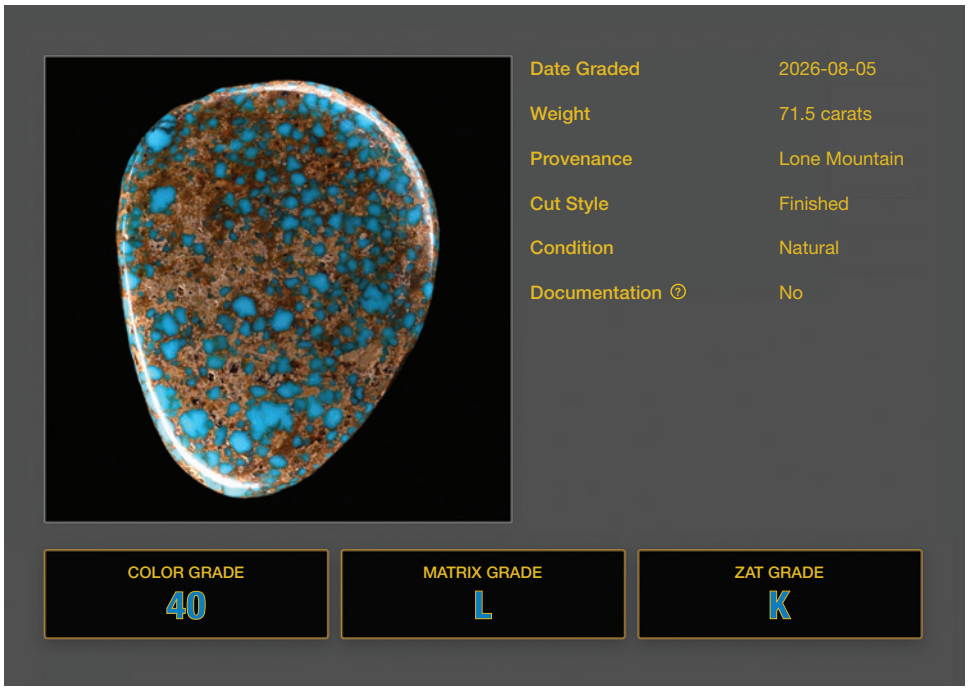

Figure 24. A partial digital grading report of a 71.5 ct natural turquoise cabochon from Lone Mountain, Nevada, receiving an official grade of 40 LK.

set. The full statistical analyses and interpretations of the studies will be submitted for peer review and publication.

Further development of the Turquoise Standard grading system is planned, including the creation of mine-specific stone sets and the expansion of the system to cover certain types of treated turquoise. Currently, grading is limited to untreated, natural loose cabochons, with a submission waitlist available at www.turquoisestandard.com.

In addition to the launch of the Turquoise Standard at the conference, the Turquoise Museum revealed plans to transition to a fully virtual museum, replacing its former physical location in Albuquerque. Scheduled to open in 2028, access to a virtual reality (VR) headset will allow turquoise enthusiasts to explore turquoise samples, stories, and mine locations from anywhere. According to Executive Director Jacob Lowry, the change will engage a new generation and provide a deeper interactive experience. Detailed 3D models of museum samples will be uploaded into the virtual environment using photogrammetric techniques. Reactions among conference attendees were mixed; some welcomed the potential wealth of accessible knowledge in the new format, while others expressed disappointment over the loss of the physical location in downtown Albuquerque.

Figure 25. This Bisbee turquoise nugget submitted by Molly Bell, weighing more than 3.5 kg, was awarded the Best in Show title at Turquoise United 2026. Photo courtesy of the Turquoise Museum.

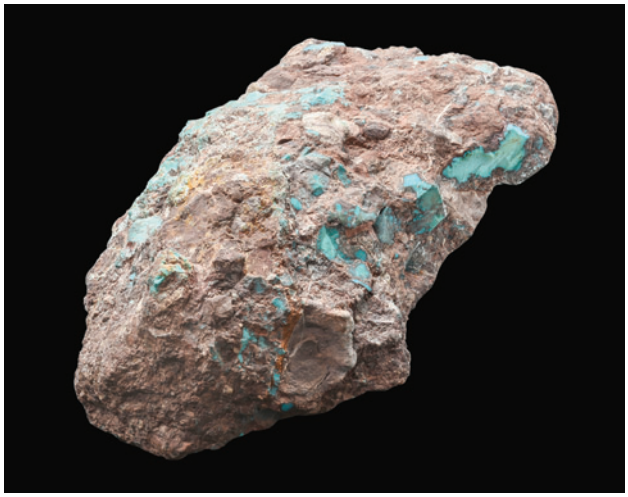

Attendees also had the opportunity to learn at Turquoise United. The author presented an overview of the history, geology, mineralogy, and treatments of turquoise on the market. Joe Dan Lowry offered a "Collecting 101" course for those interested in beginning or upgrading their turquoise collections.

Turquoise from various mines across the American Southwest, Iran, and China was available at a gem show next to the symposium hall. Exceptional specimens displayed during the gem show and conference were eligible for entry into a collection competition. Molly Bell earned Best in Show for a turquoise nugget from Bisbee, Arizona, weighing more than 3.5 kg (figure 25). Rika Hishi won a closely contested turquoise identification contest, while Mark Baca took first place in a turquoise grading challenge. The conference concluded with a banquet hosted by Ty Gibson, during which J.W. Edgar, Lynn Otteson, and Joe Dan Lowry were inducted into the Turquoise Hall of Fame.

Alexander A. Goodsuhm
GIA, Carlsbad